LJMU Research Online

Abdulqader, DA, Hathal, MS, Mahmmod, BM, Abdulhussain, SH and Al-Jumeily, D

 Plain, Edge, and Texture Detection Based on Orthogonal Moment

http://researchonline.ljmu.ac.uk/id/eprint/18569/

Article

For more information please contact researchonline@ljmu.ac.uk

RESEARCH ARTICLE

Plain, Edge, and Texture Detection Based on Orthogonal Moment

DINA A. ABDULQADER[1], **MOHAMMED SADOON HATHAL**[1], **BASHEERA M. MAHMMOD**[1], **SADIQ H. ABDULHUSSAIN**[1], **AND DHIYA AL-JUMEILY**[2], **(Senior Member, IEEE)**

[1]Department of Computer Engineering, University of Baghdad, Al-Jadriya, Baghdad 10071, Iraq
[2]School of Computer Science and Mathematics, Liverpool John Moores University, Liverpool L3 3AF, U.K.

Corresponding author: Dhiya Al-Jumeily (d.aljumeily@ljmu.ac.uk)

ABSTRACT Image pattern classification is considered a significant step for image and video processing. Although various image pattern algorithms have been proposed so far that achieved adequate classification, achieving higher accuracy while reducing the computation time remains challenging to date. A robust image pattern classification method is essential to obtain the desired accuracy. This method can be accurately classify image blocks into plain, edge, and texture (PET) using an efficient feature extraction mechanism. Moreover, to date, most of the existing studies are focused on evaluating their methods based on specific orthogonal moments, which limits the understanding of their potential application to various Discrete Orthogonal Moments (DOMs). Therefore, finding a fast PET classification method that accurately classify image pattern is crucial. To this end, this paper proposes a new scheme for accurate and fast image pattern classification using an efficient DOM. To reduce the computational complexity of feature extraction, an election mechanism is proposed to reduce the number of processed block patterns. In addition, support vector machine is used to classify the extracted features for different block patterns. The proposed scheme is evaluated by comparing the accuracy of the proposed method with the accuracy achieved by state-of-the-art methods. In addition, we compare the performance of the proposed method based on different DOMs to get the robust one. The results show that the proposed method achieves the highest classification accuracy compared with the existing methods in all the scenarios considered.

INDEX TERMS Image patterns, image properties, orthogonal polynomials, orthogonal moments, support vector machine.

I. INTRODUCTION

Nowadays, images are captured and distributed easily because of network access availability which are used extensively for business and modern communications [1]. Different image processing methods, like image acquisition, transmission, and compression, introduce various distortions to the captured image [2]. These processes affect the properties of the image (image patterns). Such properties are Plain, Texture, and Edge that are referred to as (PET). The analysis of these properties is very important since they can be used to divide the image into regions of interest, provide information about the spatial arrangement of the image, and determine the spatial distribution of intensity levels. Therefore, image patterns (PET) need to be classified accurately

The associate editor coordinating the review of this manuscript and approving it for publication was Yizhang Jiang.

based on the types of image content. Mainly, the image is partitioned into blocks and then these blocks are classified into "plain", "edge" and "texture" to be used in the desired process. For example, an image region's local quality index performance is examined for various types of distortion based on PET [2]. PET can be used to extract the discriminative features of images according to the application, where the features provide significant information about the content of an image. Such applications are perceptual visual security index [1], Content-based image quality metric [2], visible watermarking [3], quality assessment of 3D synthesized images [4], a perceptual model for jpeg applications [5], and Just Noticeable Difference Model [6], [7].

In recent years, many studies have used Discrete orthogonal moments (DOM) for digital signal processing [8]. DOM is an efficient tool that can extract significant features of the images. Different discrete transform-based

PET classification methods are performed to partition the critical areas of the image into edge block, texture block, and plain block [4]. From a mathematical point of view, DOMs are quantities that represent important features of an image, and they provide image coordinates in the orthogonal polynomial basis function [9]. In other words, the discrete transform allows the image to be viewed in the transform domain and analyzes the components of it [10]. The discrete transforms are used as feature extraction tools. Such transforms are discrete Fourier transform, discrete Wavelet transform, and discrete Walsh-Hadamard transform [11]. Transform-based techniques are used in various types of algorithms because of their powerful properties. Such algorithms are: speech enhancement [12], [13], video content analysis [14], face recognition [15], [16], and information hiding [17]. Primarily, DOMs are characterized by their energy compaction and localization properties [11]. Moments are directly defined in image coordinate space and preserve the property of moment set orthogonality. There are various types of orthogonal moments, such as Hahn moments [18], Tchebichef moments [19], [20], and Krawtchouk moments [21]. Moreover, new hybrid polynomials have been proposed recently such as: Tchebichef–Krawtchouk polynomial [9] and Krawtchouk–Tchebichef polynomial [10]. The performance of these sets exhibited noticeable merits in terms of energy compaction and localization properties [22]. These sets represent the first and second levels of the transform combination derived from discrete Tchebichef and Krawtchouk polynomials. New separable polynomials and their moments, termed as squared Tchebichef–Krawtchouk polynomials, are also proposed based on the second level of combination that achieve optimal image representation and reconstruction features [23]. These moments are based on their polynomials and extract the local features from the region of interest of an image that has unique contents (such as edges and texture). Different feature extraction classifiers have been developed using machine learning such as Support Vector Machine (SVM) which produces an accurate PET classification [24]. Typically, in image processing applications, the image's frame is partitioned into blocks to be processed separately. The robustness of feature extraction for these blocks are mainly depend on the transform properties. Where, features are stored in a memory location that corresponds to the image block to be utilized as local image descriptors [25], [26], [27], [28].

The Discrete Tchebichef Transform-based PET block classifier with an image quality metric has been proposed because different types of distortion influence various regions in the image [2]. PET classification provides good results even though the threshold values for the classification process are determined from empirical results. To overcome this issue, Tchebichef moment has been used in the image block classification based on SVM by dividing the image into non-overlapping blocks, then transforming these blocks into the moment domain to extract features that are used in the image content classification [24]. The classification has been carried out using SVM to classify the image blocks into PET blocks

(plain, edge, and texture) based on the level of moment energy with an accuracy equal to 98.7%. Although the work in this area has been presented in previous studies, different existing applications demand for accurate and fast classification of image patterns. Motivated by these issues, this work presents an accurate and fast image patterns classification method based on efficient discrete orthogonal moments.

A. CONTRIBUTIONS
The main contributions of this paper can be summarized as follows:

1) This paper considers a new mechanism for electing the blocks of plain pattern that can suppress the plain pattern blocks from further processing. The remaining blocks are passed to the next stage for more processing. This mechanism will reduce the computational time in comparison to the conventional precoding scheme.
2) Unlike previous works that have investigated the classification of image blocks using specific type of OPs, this paper investigates the use of different types of OPs through considering their powerful properties, which are essential metrics for the extracting the feature vector.
3) This paper constructs a pattern image dataset to address the task of the image patterns recognition. This dataset helps to specify the patterns of the images into plain, edge, and texture. This dataset is critically beneficial to make the classification process in different conditions.
4) Comparisons between the proposed method and the existing related works are carried our based on computational time and classification accuracy.

The rest of the paper is organized as follows. The preliminaries of the orthogonal polynomials as well as the computation of moments are introduced in Section 2. In Section 3, the methodology is presented. The experimental analysis is presented in Section 4. Finally, the conclusion is drawn in Section 5.

II. PRELIMINARIES OF THE ORTHOGONAL POLYNOMIALS
In this section, the preliminaries of the orthogonal polynomials used in this manuscript are presented. In addition, the moments computation are given.

A. DISCRETE TCHEBICHEF POLYNOMIALS (DTchPs)
The n-th order of the weighted and normalized DTchPs, which is represented by $R_n^T(x)$, is given by [29]:

$$R_n^T(x) = \frac{(1-N)_n}{\sqrt{\binom{N+n}{2n+1}(2n)!}} \, {}_3F_2 \begin{bmatrix} -x, & -n, & 1+n \\ & 1-N, & 1 \end{bmatrix}; 1 \end{bmatrix} \quad (1)$$

with

$$n = 0, 1, 2, \ldots, N-1, \text{ and}$$
$$x = 0, 1, 2, \ldots, N-1,$$

where $_pF_q(.)$ represents the generalized hypergeometric functions [30], $\binom{a}{b}$ represents the binomial coefficients, and $(\cdot)_k$ represents the Pochhammer symbol [31].

The computation of the DTchPs coefficients using hypergeometric function (1) is numerically unstable and computationally expensive [32]. Thus, to obtain stable coefficients values with low computational complexity, the recurrence algorithms are utilized [33]. Several studies have been presented and developed recurrence algorithm for DTchPs [19], [20], [29], [32]. In this paper, we have employed the recurrence algorithm in the x-direction [29]. The recurrence algorithm in the x-direction is given by:

$$R_n^T(x) = \alpha_1 R_n^T(x-1) + \alpha_2 R_n^T(x-2) \tag{2}$$

with

$$n = 0, 1, \ldots, N - 1,$$
$$x = 2, 3, \ldots, \frac{N}{2} - 1$$

where

$$\alpha_1 = -\frac{n(n+1) - (1-2x)(x-N-1) - x}{x(N-x)} \tag{3}$$

$$\alpha_2 = \frac{(x-1)(x-N-1)}{x(N-x)} \tag{4}$$

with initial values:

$$R_0^T(0) = \frac{1}{\sqrt{N}} \tag{5}$$

$$R_n^T(0) = -\sqrt{\frac{(2n+1)(N-n)}{(2n-1)(N+n)}} R_{n-1}^T(0),$$
$$n = 1, 2, \ldots, N - 1 \tag{6}$$

$$R_n^T(1) = \left(1 + \frac{n(1+n)}{1-N}\right) R_n^T(0)$$
$$n = 0, 1, \ldots, N - 1 \tag{7}$$

Additionally, to compute the rest of DTchPs coefficients, the following symmetry relation is used:

$$R_n^T(N-1-x) = (-1)^n R_n^T(x) \tag{8}$$

with

$$n = 0, 1, \ldots, N - 1$$
$$x = \frac{N}{2}, \frac{N}{2} + 1, \ldots, N - 1$$

B. DISCRETE KRAWTCHOUK POLYNOMIALS (DKraPs)
The n-th order of the weighted and normalized DKraPs, which is denoted by $R_n^K(x; p)$, based on the hypergeometric function is given by [21]:

$$R_n^K(x; p) = \sqrt{\binom{N-1}{x}\binom{N-1}{n}\left(\frac{p}{1-p}\right)^{n+x}}$$
$$\times {}_2F_1\left[\begin{matrix} -x, & -n \\ 1-N \end{matrix}; \frac{1}{p}\right] \tag{9}$$

with

$$n = 0, 1, \ldots, N - 1,$$

$$x = 0, 1, \ldots, N - 1, \text{ and}$$
$$p \in (0, 1)$$

Similar to DTchPs, to compute the DKraPs coefficient with low computation cost and without numerical error, the recurrence algorithms are utilized [8], [9], [21], [34], [35]. In this paper, we utilized the recurrence algorithm in the x-direction [9], which is given by:

$$R_n^K(x+1; p) = \frac{B}{A}R_n^K(x; p) - \frac{C}{A}R_n^K(x-1; p) \tag{10}$$

with

$$n = 0, 1, \ldots, N - 1,$$
$$x = 1, 2, \ldots, \frac{N}{2} - 2$$

with initial values:

$$R_0^K(0; p) = \sqrt{(1-p)^{N-1}} \tag{11}$$

$$R_n^K(0; p) = \sqrt{\frac{p(N-n)}{(1-p)n}} R_{n-1}^K(0; p)$$
$$n = 1, 2, \ldots, N - 1 \tag{12}$$

$$R_n^K(1; p) = \frac{p(N-1) - n}{(N-1)p}\sqrt{\frac{p(N-1)}{(1-p)}} R_n^K(0; p)$$
$$n = 0, 1, \ldots, N - 1 \tag{13}$$

where

$$A = \sqrt{(x+1)(1-p)p(N-1-x)} \tag{14}$$
$$B = x(1-p) + p(N-1-x) - n \tag{15}$$
$$C = \sqrt{p(N-x)(1-p)x} \tag{16}$$

To compute the other coefficient values of the DKraPs, the following symmetry relation is used:

$$R_n^K(x; p) = (-1)^{x+n-1} R_{N-1-n}^K(N-1-x; p) \tag{17}$$

with

$$n = 0, 1, \ldots, N - 1$$
$$x = \frac{N}{2}, \frac{N}{2} + 1, \ldots, N - 1$$

C. DISCRETE HYBRID POLYNOMIALS
Different types of combination between DTchPs and DKraPs are presented in this section, which are Discrete Krawtchouk-Tchebichef Polynomials (DKTP) [10], Discrete Tchebichef-Krawtchouk Polynomials (DKTP) [9], Discrete Squared Krawtchouk-Tchebichef Polynomials (DSKTP) [22], and Discrete Squared Tchebichef-Krawtchouk Polynomials (DSTKP) [23].

The n-th order of the hybrid forms ($R_n^{Hybrid}(x; p)$) are given in Table 1.

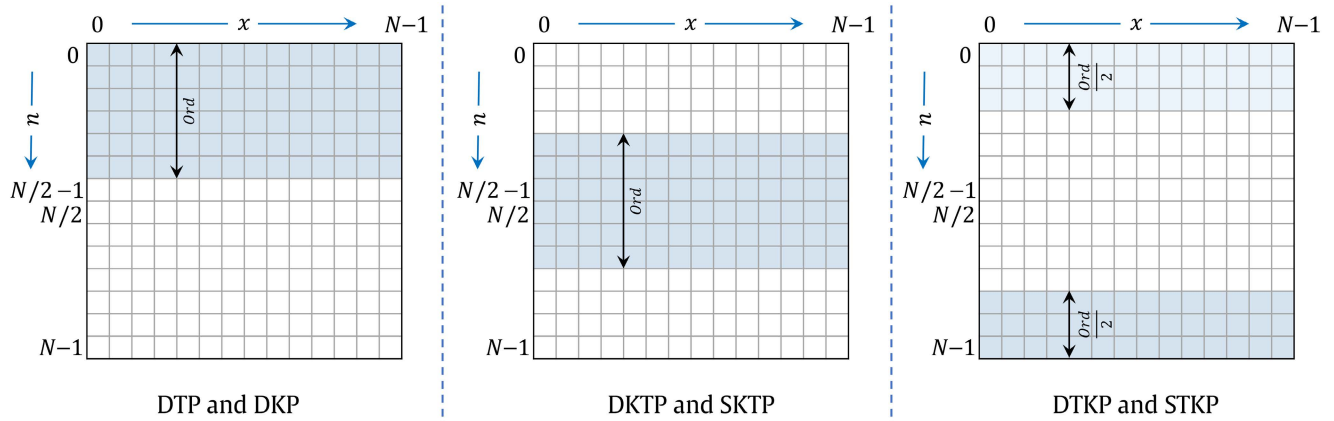In addition, the hybrid polynomial forms can be computed using matrix forms as listed in TABLE 2.

FIGURE 1. Order selection for different types of orthogonal polynomials.

TABLE 1. Mathematical representation of the discrete hybrid polynomials.

Hybrid Polynomial Name	Hybrid Polynomial Mathematical Symbol	Mathematical Form
DKTP	$R_n^{KT}(x;p)$	$\sum\limits_{i=0}^{N-1} R_i^K(n;p)R_i^T(x)$
DTKP	$R_n^{TK}(x;p)$	$\sum\limits_{i=0}^{N-1} R_i^T(n)R^K(x;p)$
SKTP	$R_n^{SKT}(x;p)$	$\sum\limits_{i=0}^{N-1}\sum\limits_{j=0}^{N-1}\sum\limits_{l=0}^{N-1} R_j^K(i;p)R_j^T(x)R_l^K(n;p)R_l^T(n)$
STKP	$R_n^{STK}(x;p)$	$\sum\limits_{i=0}^{N-1}\sum\limits_{j=0}^{N-1}\sum\limits_{l=0}^{N-1} R_j^T(i)R_j^K(x;p)R_l^T(n)R_l^K(i;p)$

TABLE 2. Representation of the discrete hybrid polynomials. Note: **tr(·)** represents matrix transpose operation.

Hybrid Polynomial Name	Hybrid Polynomial Mathematical Symbol	Mathematical Form
DKTP	$\mathbf{R^{KT}}$	$\mathbf{R^K R^T}$
DTKP	$\mathbf{R^{TK}}$	$\mathbf{tr(R^T)R^K}$
SKTP	$\mathbf{R^{SKT}}$	$\mathbf{(R^K R^T)}^2$
STKP	$\mathbf{R^{STK}}$	$\mathbf{(tr(R^T)R^K)}^2$

It is noteworthy that the set of orthogonal functions satisfy the orthogonality condition are as follows [20]:

$$\sum_{n=0}^{N-1} R_n(x)R_m(x) = \delta_{mn} = \begin{cases} 1, & n=m \\ 0, & n \neq m \end{cases} \qquad (18)$$

where δ_{nm} represents the Kronecher delta [36].

D. COMPUTATION OF MOMENTS

Discrete orthogonal moments (DOMs) are efficient tools for pattern recognition as they can extract significant features without redundancy [9], [37]. To compute the DOMs of the (n+m)th order for a 2D signal (image),$I(x, y)$, with N_y rows and N_x columns, the following formula is applied:

$$M_{nm} = \sum_{x=0}^{N_x-1} \sum_{y=0}^{N_y-1} I(x, y) R_n(x) R_m(y) \qquad (19)$$

with

$$n = 0, 1, \ldots, Ord_x$$

$$m = 0, 1, \ldots, Ord_y$$

Practically, matrix multiplication is used for fast computation in different programming environments because the Intel Math Kernel Library (MKL) is utilized [38]. In this regards, moments can be computed using matrix multiplication as follows:

$$\mathbf{M = R_y I R_x'} \qquad (20)$$

where $(\cdot)'$ represents the matrix transpose operation.

It is noteworthy that the moments need to be computed according to the order specified; this is related to the moments order (n) of the generated orthogonal polynomial. To this end, FIGURE 1 shows the order selection (Ord) for the polynomials used in this paper. More details about order selection can be found in [9], [10], [19], [22], and [23].

III. METHODOLOGY

In this section, the methodology of the image patterns (plain, edge, and texture) classification using different types of orthogonal polynomials is described.

The content of an image has various types of patterns such as plain, edge, and texture. These patterns show different moment energies in the moment domain. In addition, the moment distribution varies based on the orthogonal polynomial used. Thus, the features need to be selected carefully to obtain a high recognition rate.

In the following sections, the feature extraction is presented for each type of orthogonal polynomial, and the flow process for feature extraction and recognition is given.
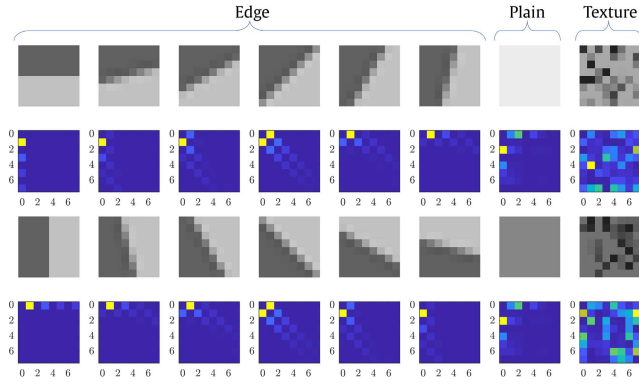
FIGURE 2. Moment energy ($M_E = M^2$) distribution for different types of patterns using DTchP.

FIGURE 3. Moment energy ($M_E = M^2$) distribution for different types of patterns using DKraP.

A. FEATURE EXTRACTION

1) FEATURE EXTRACTION FOR DTchP

FIGURE 2 shows the moment energy (M^2) distribution for an 8×8 block images of different types of patterns. The samples show edges with different angles, plains, and textures.

From FIGURE 2, it can be observed that, the plain affects the moments energy in the first row ($m = 0$ and $n = 1, 2$) and the first column ($m = 1, 2$ and $n = 0$) of the moments (M_E); While the textural information affects the entire moments. For edge information, the effect appear on the horizontal ($m = 0$ and $n = 1, 2, 3$), vertical ($m = 1, 2, 3$ and $n = 0$), and diagonal ($m = 1, 2, 3$ and $n = 1, 2, 2$) moments. Thus, the extraction of feature vector (FV_{DTchP}) can be performed as follows:

$$SSM1_{DTchP} = \sum_{n=0}^{HB^-} \sum_{m=0}^{HB^-} M_{nm}^2,$$

$$SSM2_{DTchP} = \sum_{n=0}^{HB^-} \sum_{m=HB^+}^{BS-1} M_{nm}^2$$

$$SSM3_{DTchP} \quad \sum_{n=HB^+}^{BS-1} \sum_{m=0}^{HB^-} M_{nm}^2,$$

$$SSM4_{DTchP} = \sum_{n=HB^+}^{BS-1} \sum_{m=HB^+}^{BS-1} M_{nm}^2$$

$$SSM = \left(\sum_{n=0}^{BS-1} \sum_{m=0}^{BS-1} M_{nm}^2 \right) - M_{00}^2$$

$$F_{SSM} = [SSM1_{DTchP}, SSM2_{DTchP}, SSM3_{DTchP},$$
$$\times SSM4_{DTchP}, SSM_{DTchP}]$$

$$F1_{DTchP} = \left(\sum_{m=1}^{3} M_{0m}^2 \right) / SSM1_{DTchP},$$

$$F2_{DTchP} = \left(\sum_{n=1}^{3} M_{n0}^2 \right) / SSM1_{DTchP}$$

$$F3_{DTchP} = \left(M_{11}^2 + M_{22}^2 + M_{33}^2 \right) / SSM1_{DTchP}$$

$$F4_{DTchP} = \left(M_{12}^2 + M_{13}^2 + M_{23}^2 \right) / SSM1_{DTchP}$$

$$F5_{DTchP} = \left(M_{21}^2 + M_{31}^2 + M_{32}^2 \right) / SSM1_{DTchP}$$

$$FV_{DTchP} = [F1_{DTchP}, F2_{DTchP}, F3_{DTchP}, F4_{DTchP},$$
$$\times F5_{DTchP}, F_{SSM}] \quad (21)$$

where BS represents the block size, $HB^- = \frac{N}{2} - 1$ and $HB^+ = \frac{N}{2}$.

2) FEATURE EXTRACTION FOR DKraP

The moment energy distribution for an 8×8 block images using DKraP is shown in FIGURE 3, where plain, edge, and texture patterns are shown.

From FIGURE 3, it can be observed that, the plain affects the moments energy at the indices ($m = 0$ and $n = 2, 4$), ($m = 2, 4$ and $n = 0$), and ($m = 2$ and $n = 2$); While the texture influences the entire moments. On the other hand, the edge impacts the moments at the indices ($m = 0$ and $n = 1, 2, 4$), ($m = 1, 2, 4$ and $n = 0$), ($m = 1$ and $n = 1$), ($m = 2$ and $n = 2$), and ($m = 4$ and $n = 4$). Thus, the feature vector (FV_{DKraP}) can be constructed based on the distribution of moments energy as follows:

$$SSM1_{DKraP} = \left(\sum_{n=0}^{HB^-} \sum_{m=0}^{HB^-} M_{nm}^2 \right) - M_{00}^2$$

$$SSM2_{DKraP} = \sum_{n=0}^{HB^-} \sum_{m=HB^+}^{BS-1} M_{nm}^2$$

$$SSM3_{DKraP} = \sum_{n=HB^+}^{BS-1} \sum_{m=0}^{HB^-} M_{nm}^2$$

$$SSM4_{DKraP} = \sum_{n=HB^+}^{BS-1} \sum_{m=HB^+}^{BS-1} M_{nm}^2$$

$$F_{SSMK} = [SSM1_{DKraP}, SSM2_{DKraP},$$
$$\times SSM3_{DKraP}, SSM4_{DKraP}]$$

$$F1_{DKraP} = \left(\sum_{m=1}^{4} M_{0m}^2 \right) / SSM1_{DKraP}$$

$$F2_{DKraP} = \left(\sum_{n=1}^{4} M_{n0}^2 \right) / SSM1_{DKraP}$$

FIGURE 4. Moment energy ($M_E = M^2$) distribution for different types of patterns using DKTP.
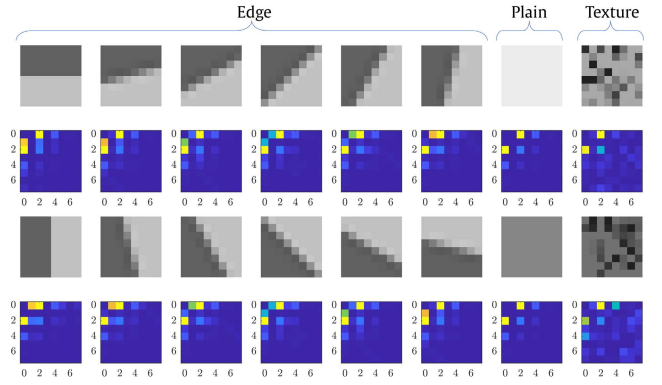

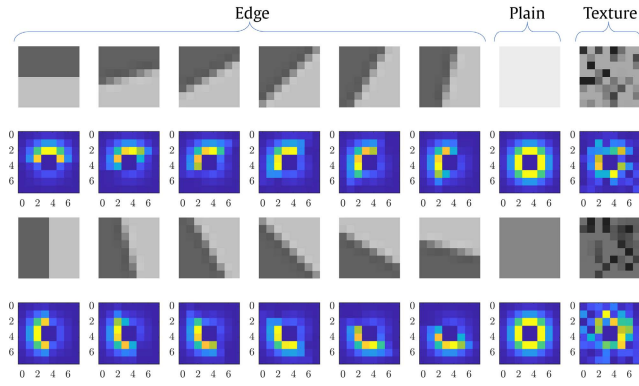**FIGURE 5.** Moment energy ($M_E = M^2$) distribution for different types of patterns using SKTP.

$$F3_{DKraP} = \left(M_{11}^2 + M_{22}^2 + M_{33}^2 + M_{44}^2\right)/SSM1_{DKraP}$$

$$F4_{DKraP} = \left(M_{12}^2 + M_{13}^2 + M_{23}^2\right)/SSM1_{DKraP}$$

$$F5_{DKraP} = \left(M_{21}^2 + M_{31}^2 + M_{32}^2\right)/SSM1_{DKraP}$$

$$F6_{DKraP} = M_{05}^2/SSM1_{DKraP}$$

$$F7_{DKraP} = M_{50}^2/SSM1_{DKraP},$$

$$F8_{DKraP} = M_{22}^2/SSM1_{DKraP}$$

$$FV_{DKraP} = [F1_{DKraP}, F2_{DKraP}, F3_{DKraP},$$
$$\times F4_{DKraP}, F5_{DKraP}, F6_{DKraP},$$
$$\times F7_{DKraP}, F8_{DKraP}, F_{SSMK}] \qquad (22)$$

$$SSM_{DKTP} = \sum_{n=1}^{6}\sum_{m=1}^{6} M_{nm}^2 - \sum_{n=3}^{4}\sum_{m=3}^{4} M_{nm}^2$$

$$F_{SSMDKT} = [SSM1_{DKTP}, SSM2_{DKTP}, SSM3_{DKTP},$$
$$\times SSM4_{DKTP}, SSM_{DKTP}]$$

$$F1_{DKTP} = [M_{22}, M_{23}, M_{24}, M_{25}]$$

$$F2_{DKTP} = [M_{25}, M_{35}, M_{45}, M_{55}]$$

$$F3_{DKTP} = [M_{32}, M_{42}]$$

$$F4_{DKTP} = [M_{35}, M_{45}]$$

$$FV_{DKTP} = [F1_{DKTP}, F2_{DKTP}, F3_{DKTP},$$
$$\times F4_{DKTP}, F_{SSMDKT}] \qquad (23)$$

3) FEATURE EXTRACTION FOR DKTP

For DKTP, the DC components are located at the center because the orders that reflect the low frequency are located at the center of the DKTP (please see FIGURE 1). Therefore, the DC components are set to zero ($n = 3, 4$ and $m = 3, 4$) and the distribution of moments for different types of image patterns with their corresponding moments energy are shown in FIGURE 4.

It can be observed that the plain impacts the moments at the center in the range ($m = 2, 5$ and $n = 2, 3, 4, 5$) and ($m = 4, 5$ and $n = 2, 5$). The texture impacts the moments outside the range ($m = 3, 4$ and $n = 3, 4$). For edge pattern, the moments influenced are in the range ($m = 1, 2, 5, 6$ and $n = 1, 2, 3, 4, 5, 6$) and ($m = 1, 2, 5, 6$ and $n = 1, 2, 3, 4, 5, 6$). Accordingly, the feature vector using DKTP (FV_{DKTP}) is derived as follows:

$$SSM1_{DKTP} = \sum_{m=2}^{5} M_{1m}^2,$$

$$SSM2_{DKTP} = \sum_{n=2}^{5} M_{n1}^2$$

$$SSM3_{DKTP} = \sum_{m=2}^{5} M_{6m}^2,$$

$$SSM4_{DKTP} = \sum_{n=2}^{5} M_{n6}^2$$

4) FEATURE EXTRACTION FOR SKTP

The moments distribution of the STKP are more compact than that of the DKTP as shown in FIGURE 5. Note that the DC components located at ($m = 3, 4$ and $n = 3, 4$) are set to zero so that the effective moments can be identified easily [2]. It can be noticed that the moments energy for all patterns are located at the center of the moments domain. However, for texture pattern, the moments are distributed in the moment domain. As a result, the features for STKP can be represented as follows:

$$SSM1_{SKTP} = \sum_{n=0}^{HB^-}\sum_{m=0}^{HB^-} M_{nm}^2$$

$$SSM2_{SKTP} = \sum_{n=0}^{HB^-}\sum_{m=HB^+}^{BS-1} M_{nm}^2$$

$$SSM3_{SKTP} = \sum_{n=HB^+}^{BS-1}\sum_{m=0}^{HB^-} M_{nm}^2$$

$$SSM4_{SKTP} = \sum_{n=HB^+}^{BS-1}\sum_{m=HB^+}^{BS-1} M_{nm}^2$$

$$F_{SSMSKT} = [SSM1_{SKTP}, SSM2_{SKTP},$$
$$\times SSM3_{SKTP}, SSM4_{SKTP}]$$

$$F1_{SKTP} = [M_{23}, M_{24}]$$

$$F2_{SKTP} = [M_{53}, M_{54}]$$

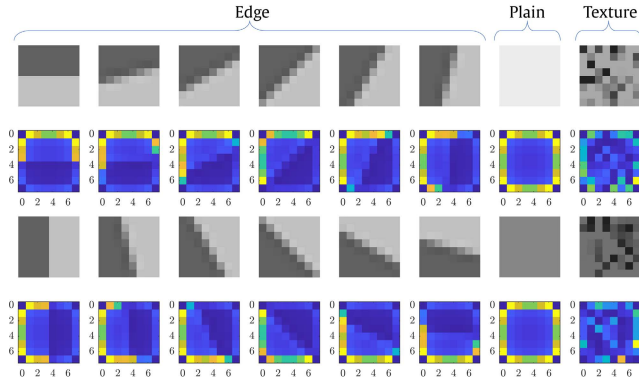**FIGURE 6.** Moment energy ($M_E = M^2$) distribution for different types of patterns using DTKP.

FIGURE 7. Moment energy ($M_E = M^2$) distribution for different types of patterns using STKP.

$$F3_{SKTP} = [M_{32}, M_{42}]$$

$$F4_{SKTP} = [M_{35}, M_{45}]$$

$$FV_{SKTP} = [F1_{SKTP}, F2_{SKTP}, F3_{SKTP},$$

$$\times F4_{SKTP}, F_{SSMSKT}] \quad (24)$$

5) FEATURE EXTRACTION FOR DTKP

For DTKP, the DC components are located at the corners because the orders that reflect the low frequency is located at the top and bottom of the DTKP plane (please see FIGURE 1). Therefore, the DC components are set to zero ($m = 0$ and $n = 0$), ($m = 0$ and $n = 7$), ($m = 7$ and $n = 0$), and ($m = 7$ and $n = 7$). The distribution of moments for different types of image patterns with their corresponding moments energy are shown in FIGURE 6.

It can be noticed that the moments energy for edge and plain patterns are located at top and bottom rows, and left and rights columns. However, for texture pattern, the moments are spread at various locations of the moment domain. Therefore, the features for DTKP can be derived as follows:

$$SSM1_{DTKP} = \left(\sum_{n=0}^{HB^-} \sum_{m=0}^{HB^-} M_{nm}^2 \right) - M_{00}^2,$$

$$SSM2_{DTKP} = \left(\sum_{n=0}^{HB^-} \sum_{m=HB^+}^{BS-1} M_{nm}^2 \right) - M_{07}^2$$

$$SSM3_{DTKP} = \left(\sum_{n=HB^+}^{BS-1} \sum_{m=0}^{HB^-} M_{nm}^2 \right) - -M_{70}^2,$$

$$SSM4_{DTKP} = \left(\sum_{n=HB^+}^{BS-1} \sum_{m=HB^+}^{BS-1} M_{nm}^2 \right) - M_{77}^2$$

$$F_{SSMTK} = [SSM1_{DTKP}, SSM2_{DTKP},$$

$$\times SSM3_{DTKP}, SSM4_{DTKP}]$$

$$F1_{DTKP} = [M_{01}, M_{02}, M_{03}, M_{04}, M_{05}, M_{06}]$$

$$F2_{DTKP} = [M_{10}, M_{20}, M_{30}, M_{40}, M_{50}, M_{60}]$$

$$F3_{DTKP} = [M_{71}, M_{72}, M_{73}, M_{74}, M_{75}, M_{76}]$$

$$F4_{DTKP} = [M_{17}, M_{27}, M_{37}, M_{47}, M_{57}, M_{67}]$$

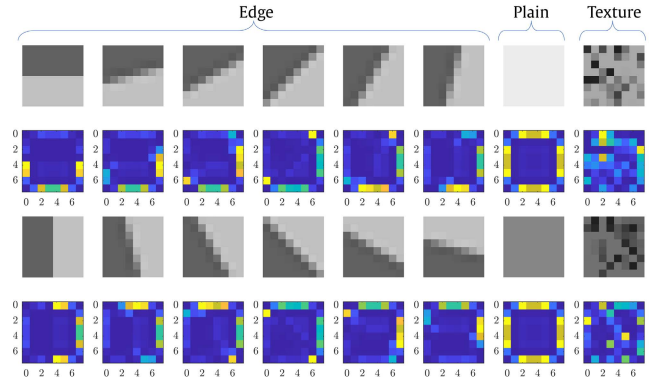$$FV_{DTKP} = [F1_{DTKP}, F2_{DTKP}, F3_{DTKP},$$

$$\times F4_{DTKP}, F_{SSMTK}] \quad (25)$$

6) FEATURE EXTRACTION FOR STKP

FIGURE 7 shows the moment distribution of the STKP. It is easily observed that the moments that are influenced by the plain, edge, and texture patterns are similar to those of the DTKP. However, the moments energies are different from that of the DTKP. Therefore, the features that need to be extracted for the STKP are similar to those of the DTKP.

The scaling of features is considered an important step to obtain a similar range of independent variables which is strongly influences the recognition rate [39]. In this work, feature scaling used in this work is by mapping the mean ($mean(FV)$) and standard deviation ($std(FV)$) of the feature vector into $mean_t$ and std_t, respectively, as follows:

$$FV_s = (FV - mean(FV)) \cdot \frac{std_t}{std(FV)} + mean_t \quad (26)$$

where FV_s denotes the scaled feature vector, FV represents one of the feature vectors extracted previously based on the polynomial used. The values of $mean_t$ and std_t are set to 0 and 1, respectively.

B. THE ELECTED PLAIN PATTERNS

Generally, an image contains the three image patterns (plain, edge, and texture). Each image has multiple plain patterns where their total number is non-zero. In addition, the pixel intensities of plain patterns show high similarity, i.e., very small changes in the pixel intensities. On the other hand, the values of the pixel intensities for edge and texture patterns show noticeable changes. In this work, we have presented a method for electing the blocks of plain patterns and the rest of the blocks are passed to the next stage, i.e., classification stage. The aim of this stage is to eliminate the plain patterns which will minimize the computation time. Thus, a block with a high similarity between pixels intensities is considered as a plain pattern. While, the rest of the blocks are passed to the next stage for further processing. In the next stage, the image blocks that are judged as non-plain patterns will be processed. The processing will involve computing moments,
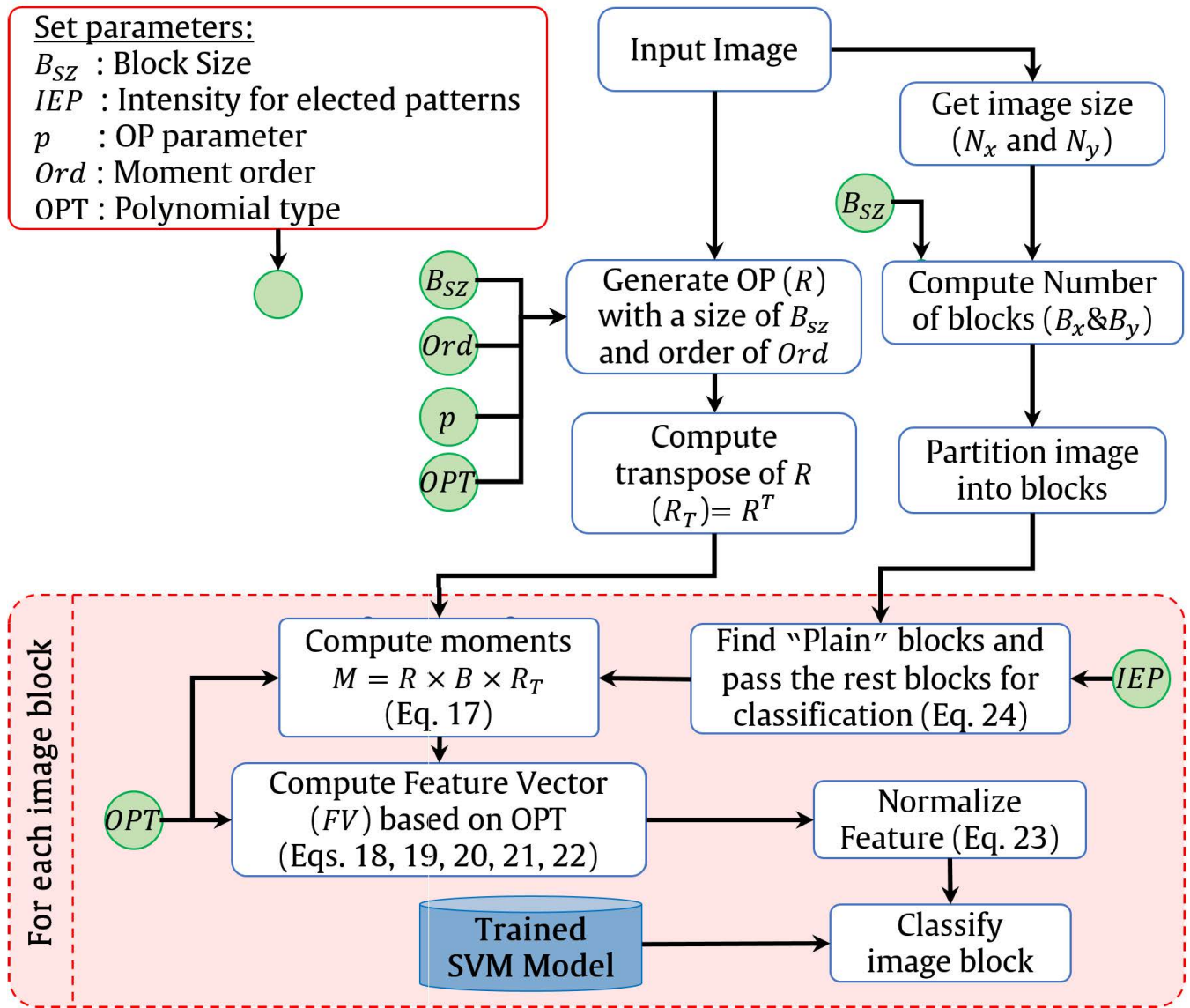
FIGURE 8. A diagram for the procedure of the presented algorithm to predict the image patterns.

constructing the feature vector, and predicting the pattern of the image block (plain, edge, or texture). This is applied when the difference between the maximum and minimum pixel intensities is greater than *IEP* (please see FIGURE 8) as follows:

$$EP = \begin{cases} 1; & (\max(I) - \min(I)) > IEP \\ 0; & otherwise \end{cases} \quad (27)$$

where *EP* represents the elected pattern, *IEP* is the intensity threshold for elected patterns, $\min(I)$ and $\max(I)$ return the minimum and maximum intensity values from the image block. For more elucidation, the pseudo code for elected pattern mechanism is presented in Algorithm 1. Note that the best value of IEP is experimentally found to be 0.1 in double precision format or 25 in unsigned integer.

C. THE IMAGE PATTERN CLASSIFICATION
Now, the type of image patterns need to be predicted after the feature vector has been extracted and normalized. In this paper, support vector machine (SVM) is used for classification. The LIB-SVM is employed in this paper with radial basis function (RBF) as a kernel function [39], [40]. The RBF kernel is selected because of the effective classification mechanism since the RBF kernel shows nonlinear separation between classes [39]. FIGURE 8 depicts the diagram of the procedure used to predict the pattern of images.

IV. EXPERIMENTAL RESULTS
In this section, the generated dataset and its procedure are presented. In addition, the training and testing procedures are presented. Finally, the experimental analysis of the presented work is given.

Algorithm 1 The Proposed Mechanism for Electing Plain Patterns

Input: I=image block, IEP=Intensity for electing pattern.
Output: EP = Elected pattern.

1: $a = \max(I)$ {Return the maximum intensity value in the image block I.}
2: $b = \min(I)$ {Return the minimum intensity value in the image block I.}
3: $I_\Delta = b - a$ {Find the difference between the maximum and minimum intensities.}
4: **if** $I_\Delta > IEP$ **then**
5:   $EP = 1$ {Non Plain pattern. This image block is passed to the next stage.}
6: **else**
7:   $EP = 0$ {Elected as Plain pattern.}
8: **end if**
9:
10: **return** EP

A. DETAILS OF THE DATASET

The dataset of the existing works is very small. For example, [24] has selected manually 150 images for each pattern. However, the dataset is considered small to predict the various angles and cases for edge pattern. In this paper, we have generated 1080, 1800, 3600 for edge, plain, and texture patterns respectively. In addition, the generated edge patterns are degraded by Gaussian noise to discover the effect of illumination change. Thus, the total generated patterns are 7560.

Algorithm 2 The Generation of Plain Pattern Images of the Dataset

Input: BS=Block size, $minI$=minimum intensity, $maxI$=maximum intensity.
Output: Plain patterns.

1: P_{ind}=0 {▷ P_{ind} represents the index used for storing} the Plain images in a cell array
2: **for** $i \leftarrow 1$ to T_{plain} **do**
   {▷T_{plain} denotes the required number of plain} images and it is set to 1800.
3:   $P_{ind} \leftarrow P_{ind} + 1$
4:   Plain(P_{ind})$\leftarrow [J_{BS}] \cdot (i/int_{control})$ {▷ $int_{control}$ is used to control the intensity values.}
5: **end for**
6: **return** Plain pattern images

For the testing dataset, different values of $int_{control}$ (in Algorithm 2 and Algorithm 3) have been used such that the intensity of plain and texture values are distinct from the training set. For edge patterns, the image patterns are generated with a size of 16×16 and with 6 shifts. Then, the images of the edge patterns are resized into 8×8 images, which will produce images with a blurry edge pattern. Moreover, the generated edge patterns are degraded by a Gaussian noise which will produce (($angles = 360$) $\times$ ($shifts = 6$) $\times$ ($clean$ and $noisy = 2$) $= 4320$). For texture patterns, the

Algorithm 3 The Generation of Texture Pattern Images of the Dataset

Input: BS=Block size, $minI$=minimum intensity, $maxI$=maximum intensity.
Output: Texture patterns.

1: $T_{ind} \leftarrow 0$ {▷T_{ind} represents the index used for storing the} Texture images in a cell array
2: **for** $i \leftarrow 1$ to T_{Tex} **do**
   {▷ T_{Tex} represents the total number of texture} images and it is set to 3600.
3:   $T_{ind} \leftarrow T_{ind} + 1$
4:   Texture(T_{ind}) $\leftarrow$ [$U(BS)$] $\cdot$ ($i/int_{control}$) {▷generate a matrix of size $BS \times BS$ with} uniformly distributed random numbers.
5: **end for**
6: **return** Texture pattern images

TABLE 3. The details of the train and test datasets.

Dataset	Edge	Plain	Texture	Total
Train	2160	1800	3600	7560
Test	4320	3600	3600	11520

number of generated images is 3600; while for plain patterns, the number of generated clean images is 1800 and for noisy plain patterns degraded by Gaussian noise is 1800. Thus, the total number of images in the test dataset is 11520. A summary of the train and test dataset are given in TABLE 3.

B. PERFORMANCE EVALUATION OF SVM KERNELS

The aim of the presented work is to predict the image patterns correctly and achieve a high recognition rate. In this study, the MATLAB code of LIBSVM [40] toolbox was used for classification. The classification process using the SVM includes training and testing process. The C-type of the SVM technique with radial basis function was used for training. These choices are considered as an effective classification mechanism. This kernel shows nonlinear separation between classes. To ensure high prediction accuracy, the cross-validation process is carried out to obtain the best kernel parameters. Note that the cost and gamma are essential parameters that need to be tuned with applying five-fold cross-validation. The ranges of the parameters for cost and gamma are considered to be $(2^0, 2^1, \ldots, 2^5)$ and $(2^{-10}, 2^{-9}, \ldots, 2^0)$. The cost and gamma parameters show high accuracy on the testing set. To justify the selection of the RBF kernel, we have tested the presented algorithm using three kernels: 1) linear, 2) polynomial, and 3) RBF. The results of this test phase are shown in TABLE 4. It should be noted that the dataset presented in this work (Section IV-A)is used to obtain the results in TABLE 4.

The results in TABLE 4 show that the average recognition rate of RBF kernel is 11.2% more than the linear kernel; while it is greater than polynomial kernel by 0.75%. Consequently, RBF is utilized as a kernel for the SVM because the recognition rate for the RBF kernel is higher than other SVM kernels (linear and polynomial).

FIGURE 9. Test images of size 480 × 704 and their corresponding elected patterns. Image from top left to bottom right: "sailing2", "womanhat", "statue", and "sailing3".
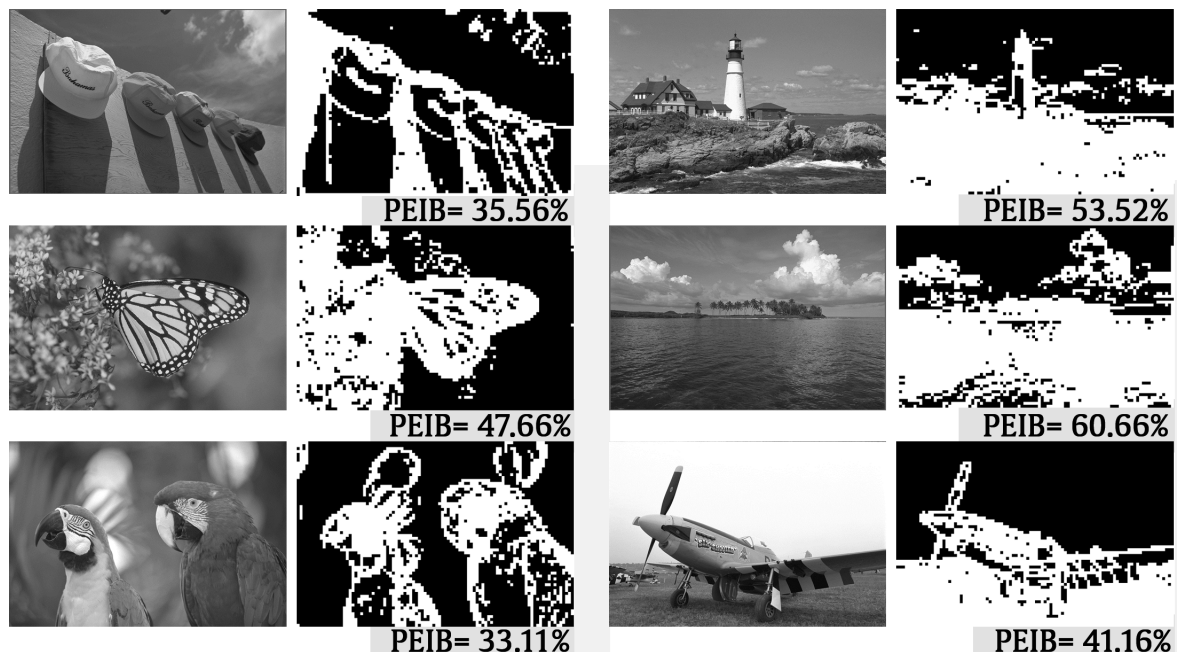

FIGURE 10. Test images of size 768 × 512 and their corresponding elected patterns. Image from top left to bottom right: "caps", "lighthouse2", "monarch", "ocean", "parrots", and "plane".

C. COMPARISON WITH EXISTING WORKS

In this section, the performance of the presented algorithm is evaluated. The evaluation is carried out in terms of recognition rate (accuracy), and computation cost. In addition, visual inspection has been presented.

In the presented algorithm, we utilize SVM as a classifier with the RBF as a kernel. The comparison is performed with two previous studies: image pattern classification based on threshold rules (PCTR) [2] and image pattern classification based on SVM (PCSV) [24]. The proposed work is compared
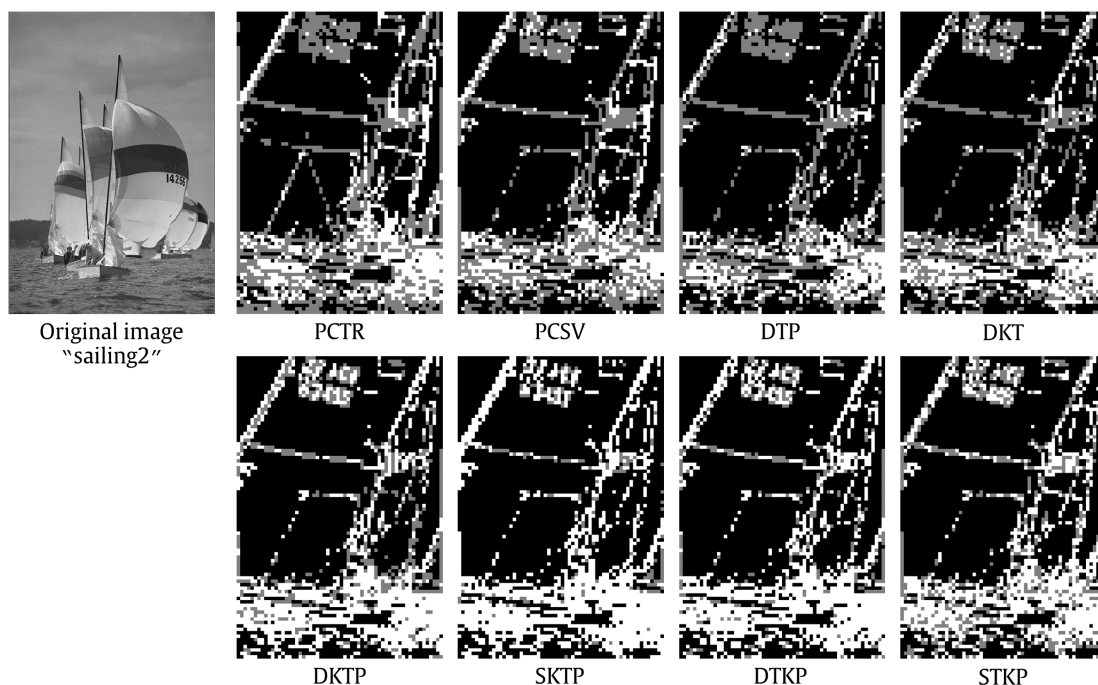
FIGURE 11. Results of the test image "sailing2" carried out using the proposed and existing algorithms.
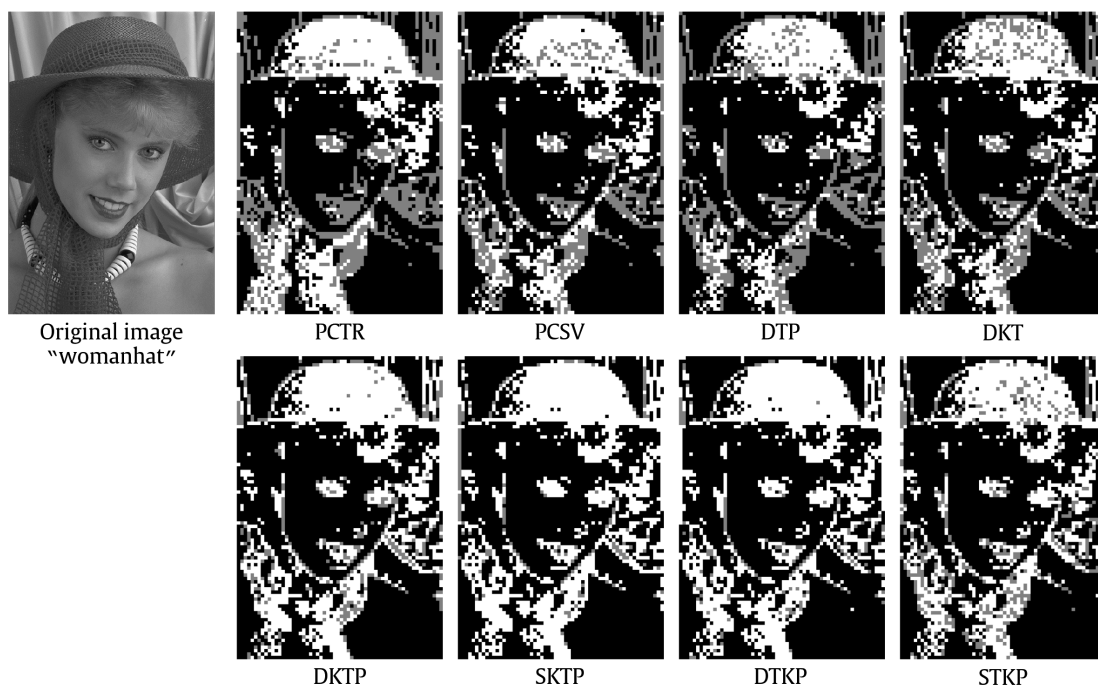
FIGURE 12. Results of the test image "womanhat" carried out using the proposed and existing algorithms.

with PCTR and PCSV because these works are considered the most related existing works that need more insight to be more accurate and faster in the image pattern classification. It is noteworthy that the PCTR and PCSV perform the pattern classification using DTchP only. TABLE 5 shows the recognition rate of the presented algorithm and the existing methods (PCTR and PCSV).

The reported results reveal that the PCTR [2] attains the recognition rate of 88.32% which is the minimum recognition level. While the PCSV [24] shows better recognition rate than

Algorithm 4 The Generation of the Edge Pattern Images of the Dataset

Input: BS=Block size, $minI$=minimum intensity, $maxI$=maximum intensity.

Output: Edge patterns.

1: $E_{ind} \leftarrow 0$ {▷ E_{ind} represents the index used for storing} the Edge images in a cell array
2: **for** $i \leftarrow 1$ to $Angles$ **do**
  {▷ $Angles$ represents the angles to be gener-}
  ated. Since we will reverse (in step 19) the
  generated Edge image, the values of $Angles$
  is set to 180.
3: $E_{ind} \leftarrow E_{ind} + 1$
4: Temp=$[J_{BS/2,BS} \cdot minI \; ; J_{BS/2,BS} \cdot maxI]$
5: Temp←rotate(Temp, i) {▷The rotated image are cropped.}
6: Edge(E_{ind})←Temp
7: $E_{ind} \leftarrow E_{ind} + 1$
8: Edge(E_{ind}) ← RE(Edge($E_{ind} - 1$)) {▷RE represents reversing the elements in each row.}
9: **for** $j \leftarrow 1$ to 2 **do**
  {▷j represents shift in angle}
10: **if** $i <45$ **then**
11: Edge($E_{ind} + j$) ← SU(Edge(E_{ind})) {▷SU denotes shift the edge up.}
12: **else if** $i \geq 45$ and $i <136$ **then**
13: Edge($E_{ind} + j$) ← SL(Edge(E_{ind})) {SL denotes shift the edge left.}
14: **else**
15: Edge($E_{ind} + j$) ← SR(Edge(E_{ind})) {▷SR denotes shift the edge right.}
16: **end if**
17: $E_{ind} = E_{ind} + 1$
18: Edge($E_{ind} + 1$) ← RE(Edge(E_{ind}))
19: $E_{ind} = E_{ind} + 1$
20: **end for**
21: **end for**
22: **return** Edge image patterns

TABLE 4. Recognition rates (%) of patterns for different types of SVM kernels.

Orthogonal	SVM Kernel		
Polynomial	Linear	Polynomial	RBF
DTchP	93.44	97.47	97.62
DKraP	97.31	97.03	97.86
DKTP	84.03	97.61	99.48
SKTP	86.12	98.65	99.01
STKP	82.07	97.85	99.04
SKTP	82.77	98.72	98.85
Average	87.62	97.89	98.64

PCTR with an improvement of 2.54%. On the other hand, the results of the presented algorithm outperforms the existing algorithms with improvement ranging 8.62% to 9.3%. The DKTP has achieved the best recognition rate among other types of orthogonal polynomials.

TABLE 5. Recognition rate of the presented algorithm and existing algorithms using the test dataset.

Algorithm	Accuracy					
	DTchP	DKraP	DKTP	SKTP	DTKP	STKP
PCTR [2]	88.32	-	-	-	-	-
PCSV [24]	90.86	-	-	-	-	-
Ours	97.62	97.86	99.48	99.01	99.04	98.85

TABLE 6. Computation time of the presented and existing algorithm using the image "womanhat" from Live dataset [41].

Algorithm	Computation time					
	DTchP	DKraP	DKTP	SKTP	DTKP	STKP
PCTR [2]	0.521	-	-	-	-	-
PCSV [24]	1.252	-	-	-	-	-
Ours without elected patterns	0.616	0.976	2.074	0.884	4.540	4.446
Ours with elected patterns	0.275	0.416	0.847	0.382	1.805	1.778
Elected pattern improvement	2.24	2.35	2.45	2.31	2.52	2.50

The performance of the presented algorithm and existing works was determined in terms of computational time. Moreover, to show the effect of the elected plain on the computation time, we have carried out the experiment for the presented algorithm without and with the elected patterns technique. TABLE 6 summarizes the obtained results. The results of the computation time reveal that the computation time increases as the number of extracted features increases. Also, it is clear that the proposed algorithm with the elected pattern technique has an average improvement of 2.39 [1] over the presented algorithm without the elected pattern technique. Compared with the existing algorithm, the presented algorithms using DTchP, DKraP, and SKTP is faster than PCTR [2] and PCSV [24]. However, the presented algorithm using DKTP is also faster than PCSV [24].

To show the impact of the elected pattern technique, an experiment is performed using the Live dataset [41] on two groups of images. The first test is performed on images with a size of 480×704 and the results are depicted in FIGURE 9. The results show that the black pixels are the blocks with plain pixel; while the white pixels represent the blocks of the pixels that will be passed to the next stage to be recognized as one of the image patterns (plain, edge, and texture).

In addition, the experiment is performed for a group of images with a size of 768×572 and the results are shown in FIGURE 10. The percentage of the elected image blocks (PEIB), white pixels in Figures 9 and 10, is computed and placed under the images. The PEIB is computed as follows:

$$PEIB = \frac{Number \; of \; elected \; pixels}{Total \; number \; of \; pixels} \times 100\% \quad (28)$$

---

[1]This value represents the average of the elected pattern improvement extracted from TABLE 6.

It can be noticed from the values of PEIB is that the percentage of the pixels to be processed to the total number of pixel is $\sim 48\%$ [2]

For visual inspection, we have carried out an experiment using the proposed and existing algorithm on two images from the Live dataset. The results of the experiment on the "sailing" image are shown in FIGURE 11 and the results of the "womanhat" are shown in FIGURE 12.

V. CONCLUSION

This paper proposed a new method for finding a fast and accurate image pattern classification method. A robust image pattern recognition method is designed to meet the desired recognition accuracy by extracting the features efficiently and classifying the image blocks into plain, edge, and texture (PET) based on the codesign of different types of discrete orthogonal polynomials with their associated moments. An election mechanism was proposed to reduce the computational complexity of the feature extraction by reducing the number of processed block patterns. In addition, SVM is used to classify the extracted features for the different patterns accurately. The proposed method was evaluated by comparing the accuracy of the proposed method with the accuracy achieved using the existing methods and comparing the performance of the proposed method for different types of DOM to get the most robust one. The results demonstrated that the proposed approach achieved the highest recognition accuracy with low computational complexity when compared with the state-of-the-art methods. Although this work outperforms existing algorithms, it is only applied to Grayscale images. Thus, future work may consider the investigation of performing image pattern classification for color images.

REFERENCES

[1] T. Xiang, S. Guo, and X. Li, "Perceptual visual security index based on edge and texture similarities," *IEEE Trans. Inf. Forensics Security*, vol. 11, no. 5, pp. 951–963, May 2016.

[2] K.-H. Thung, R. Paramesran, and C.-L. Lim, "Content-based image quality metric using similarity measure of moment vectors," *Pattern Recognit.*, vol. 45, no. 6, pp. 2193–2204, 2012.

[3] A. Cedillo-Hernandez, M. Cedillo-Hernandez, F. Garcia-Ugalde, M. Nakano-Miyatake, and H. Perez-Meana, "A visible watermarking with automated location technique for copyright protection of portrait images," *IEICE Trans. Inf. Syst.*, vol. 99, no. 6, pp. 1541–1552, 2016.

[4] X. Wang, F. Shao, Q. Jiang, R. Fu, and Y.-S. Ho, "Quality assessment of 3D synthesized images via measuring local feature similarity and global sharpness," *IEEE Access*, vol. 7, pp. 10242–10253, 2019.

[5] H. H. Y. Tong and A. N. Venetsanopoulos, "A perceptual model for JPEG applications based on block classification, texture masking, and luminance masking," in *Proc. Int. Conf. Image Process. (ICIP)*, vol. 3, Oct. 1998, pp. 428–432.

[6] W. Wan, J. Wu, X. Xie, and G. Shi, "A novel just noticeable difference model via orientation regularity in DCT domain," *IEEE Access*, vol. 5, pp. 22953–22964, 2017.

[7] H. Wang, L. Yu, H. Yin, T. Li, and S. Wang, "An improved DCT-based JND estimation model considering multiple masking effects," *J. Vis. Commun. Image Represent.*, vol. 71, Aug. 2020, Art. no. 102850.

[8] S. H. Abdulhussain, A. R. Ramli, S. A. R. Al-Haddad, B. M. Mahmmod, and W. A. Jassim, "Fast recursive computation of Krawtchouk polynomials," *J. Math. Imag. Vis.*, vol. 60, no. 3, pp. 285–303, 2018.

[9] W. A. Jassim, P. Raveendran, and R. Mukundan, "New orthogonal polynomials for speech signal and image processing," *IET Signal Process.*, vol. 6, no. 8, pp. 713–723, Oct. 2012.

[10] B. M. Mahmmod, A. R. B. Ramli, S. H. Abdulhussain, S. A. R. Al-Haddad, and W. A. Jassim, "Signal compression and enhancement using a new orthogonal-polynomial-based discrete transform," *IET Signal Process.*, vol. 12, no. 1, pp. 129–142, Aug. 2018.

[11] S. H. Abdulhussain, S. A. R. Al-Haddad, M. I. Saripan, B. M. Mahmmod, and A. Hussien, "Fast temporal video segmentation based on Krawtchouk-Tchebichef moments," *IEEE Access*, vol. 8, pp. 72347–72359, 2020.

[12] B. M. Mahmmod, A. R. Ramli, S. H. Abdulhussain, S. Al-Haddad, and W. A. Jassim, "Low-distortion MMSE speech enhancement estimator based on Laplacian prior," *IEEE Access*, vol. 5, pp. 9866–9881, 2017.

[13] B. M. Mahmmod, A. R. Ramli, T. Baker, F. Al-Obeidat, S. H. Abdulhussain, and W. A. Jassim, "Speech enhancement algorithm based on super-Gaussian modeling and orthogonal polynomials," *IEEE Access*, vol. 7, pp. 103485–103504, 2019.

[14] S. H. Abdulhussain, B. M. Mahmmod, M. I. Saripan, S. A. R. Al-Haddad, T. Baker, W. N. Flayyih, and W. A. Jassim, "A fast feature extraction algorithm for image and video processing," in *Proc. Int. Joint Conf. Neural Netw.*, Jul. 2019, pp. 1–8.

[15] S. H. Abdulhussain, B. M. Mahmmod, A. AlGhadhban, and J. Flusser, "Face recognition algorithm based on fast computation of orthogonal moments," *Mathematics*, vol. 10, no. 15, p. 2721, Aug. 2022.

[16] F. Akhmedova and S. Liao, "Face recognition with discrete orthogonal moments," in *Recent Advances in Computer Vision*. Springer, 2019, pp. 189–209.

[17] H. S. Radeaf, B. M. Mahmmod, S. H. Abdulhussain, and D. Al-Jumaeily, "A steganography based on orthogonal moments," in *Proc. Int. Conf. Inf. Commun. Technol. (ICICT)*, New York, NY, USA, 2019, pp. 147–153.

[18] P. T. Yap, R. Paramesran, and S. H. Ong, "Image analysis using Hahn moments," *IEEE Trans. Pattern Anal. Mach. Intell.*, vol. 29, no. 11, pp. 2057–2062, Nov. 2007.

[19] S. H. Abdulhussain, A. R. Ramli, S. A. R. Al-Haddad, B. M. Mahmmod, and W. A. Jassim, "On computational aspects of tchebichef polynomials for higher polynomial order," *IEEE Access*, vol. 5, pp. 2470–2478, 2017.

[20] R. Mukundan, S. H. Ong, and P. A. Lee, "Image analysis by Tchebichef moments," *IEEE Trans. Image Process.*, vol. 10, no. 9, pp. 1357–1364, Sep. 2001.

[21] P. T. Yap, R. Paramesran, and S.-H. Ong, "Image analysis by Krawtchouk moments," *IEEE Trans. Image Process.*, vol. 12, no. 11, pp. 1367–1377, Nov. 2003.

[22] S. H. Abdulhussain, A. R. Ramli, B. M. Mahmmod, M. I. Saripan, S. A. R. Al-Haddad, and W. A. Jassim, "A new hybrid form of Krawtchouk and Tchebichef polynomials: Design and application," *J. Math. Imag. Vis.*, vol. 61, no. 4, pp. 555–570, 2019.

[23] Z. N. Idan, S. H. Abdulhussain, and S. A. R. Al-Haddad, "A new separable moments based on Tchebichef-Krawtchouk polynomials," *IEEE Access*, vol. 8, pp. 41013–41025, 2020.

[24] C.-L. Lim, K.-H. Thung, Y.-P. Yu, S.-L. Wong, and P. Raveendran, "Plain, edge, texture (PET) block classifier using tchebichef moments and SVM," in *Proc. Int. Symp. Intell. Signal Process. Commun. Syst.*, Nov. 2013, pp. 409–412.

[25] S. H. Abdulhussain, B. M. Mahmmod, J. Flusser, K. A. Al-Utaibi, and S. M. Sait, "Fast overlapping block processing algorithm for feature extraction," *Symmetry*, vol. 14, no. 4, p. 715, Apr. 2022.

[26] B. A. Hussain and M. S. Hathal, "Development of Iraqi license plate recognition system based on Canny edge detection method," *J. Eng.*, vol. 26, no. 7, pp. 115–126, Jul. 2020.

[27] H. K. Abbas, A. H. Al-Saleh, H. J. Mohamad, and A. A. Al-Zuky, "New algorithms to enhanced fused images from auto-focus images," *Baghdad Sci. J.*, vol. 18, no. 1, p. 0124, 2021.

[28] S. H. Abdulhussain, A. R. Ramli, A. J. Hussain, B. M. Mahmmod, and W. A. Jassim, "Orthogonal polynomial embedded image kernel," in *Proc. Int. Conf. Inf. Commun. Technol. (ICICT)*, New York, NY, USA, 2019, pp. 215–221.

[29] R. Mukundan, "Some computational aspects of discrete orthonormal moments," *IEEE Trans. Image Process.*, vol. 13, no. 8, pp. 1055–1059, Aug. 2004.

---

[2]This value represents the average of PEIB of the test images in Figures 9 and 10. This clearly shows that the image blocks that will be fed to the next stage to be processed in the next stage are significantly reduced, which means that the computation time will be reduced to more than 50%.

[30] J. P. Hannah, "Identities for the gamma and hypergeometric functions: An overview from Euler to the present," M.S. thesis, Univ. Witwatersrand, 2013.

[31] J. J. Foncannon, "Irresistible integrals: Symbolics, analysis and experiments in the evaluation of integrals," *Math. Intell.*, vol. 28, no. 3, pp. 65–68, 2006.

[32] C. Camacho-Bello and J. S. Rivera-Lopez, "Some computational aspects of tchebichef moments for higher orders," *Pattern Recognit. Lett.*, vol. 112, pp. 332–339, Sep. 2018.

[33] H. Zhu, M. Liu, H. Shu, H. Zhang, and L. Luo, "General form for obtaining discrete orthogonal moments," *IET Image Process.*, vol. 4, no. 5, p. 335, 2010.

[34] B. M. Mahmmod, A. M. Abdul-Hadi, S. H. Abdulhussain, and A. Hussien, "On computational aspects of Krawtchouk polynomials for high orders," *J. Imag.*, vol. 6, no. 8, p. 81, Aug. 2020.

[35] K. A. Al-Utaibi, S. H. Abdulhussain, B. M. Mahmmod, M. A. Naser, M. Alsabah, and S. M. Sait, "Reliable recurrence algorithm for high-order Krawtchouk polynomials," *Entropy*, vol. 23, no. 9, p. 1162, Sep. 2021.

[36] G. Zhang, Z. Luo, B. Fu, B. Li, J. Liao, X. Fan, and Z. Xi, "A symmetry and bi-recursive algorithm of accurately computing Krawtchouk moments," *Pattern Recognit. Lett.*, vol. 31, no. 7, pp. 548–554, May 2010.

[37] H. Abbas and L. E. George, "Image classification schemes based on sliced radial energy distribution of DFT and the statistical moments of Haar wavelet," *Iraqi J. Sci.*, pp. 687–712, Mar. 2020.

[38] Z. Rinkevicius, "VeloxChem: A Python-driven density-functional theory program for spectroscopy simulations in high-performance computing environments," *Wiley Interdiscipl. Rev., Comput. Mol. Sci.*, vol. 10, no. 5, p. e1457, 2020.

[39] C.-W. Hsu, C.-C. Chang, and C.-J. Lin, "A practical guide to support vector classification," Dept. Comput. Sci. Inf. Eng., Tech. Rep., 2003.

[40] C. Chang and C. Lin, "LIBSVM," *ACM Trans. Intell. Syst. Technol.*, vol. 2, no. 3, pp. 1–27, 2011.

[41] L. Sheikh, H. R. Wang, and Z. Cormack. (2010). *Live Image Quality Assessment Database Release 2*. [Online]. Available: http://live.ece.utexas.edu/research/quality

DINA A. ABDULQADER received the B.Sc. and M.Sc. degrees in computer engineering from Baghdad University, Iraq, in 2006 and 2012, respectively. Since 2007, she has been a Faculty Member with the University of Baghdad. Her research interests include image processing, machine learning, and signal processing.

MOHAMMED SADOON HATHAL received the B.Sc. and M.Sc. degrees in computer engineering from the University of Technology, Baghdad, Iraq, and the Ph.D. degree in software engineering from University Sains Malaysia, Penang, Malaysia. He was a Postdoctoral Researcher at the Luleå University of Technology, Lulea, Sweden. Currently, he is a Lecturer with the School of Computer Engineering, University of Baghdad. His research interests include microwave imaging, medical imaging, computer algorithms, biometric security, the Internet of Things, deep learning, intelligent systems, and software design and development.

BASHEERA M. MAHMMOD received the Ph.D. degree in computer and embedded system engineering from UPM, in 2018. She is currently a Lecturer at the Department of Computer Engineering, University of Baghdad. Her research interests include signal processing, speech enhancement, and computer vision.
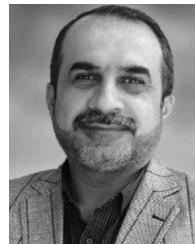
SADIQ H. ABDULHUSSAIN received the Ph.D. degree in computer and embedded system engineering from UPM, in 2018. Since 2008, he has been a Faculty Member with the University of Baghdad. His research interests include image processing, computer vision, and signal processing.

DHIYA AL-JUMEILY (Senior Member, IEEE) is currently a Professor in artificial intelligence and the President of eSystems Engineering Society. He has published well over 300 peer-reviewed scientific international publications, 12 books and 14 book chapters, in multidisciplinary research areas, including machine learning, neural networks, signal prediction, telecommunication fraud detection, AI-based clinical decision-making, medical knowledge engineering, human–machine interaction, intelligent medical information systems, sensors and robotics, wearable and intelligent devices, and instruments. He has extensive research interests include a wide variety of interdisciplinary perspectives concerning the theory and practice of applied artificial intelligence in medicine, human biology, environment, intelligent community, and health care. But, his current research passion is decision support systems for self-management of health and medicine. He has successfully supervised over 20 Ph.D. student's studies and has been an external examiner to various U.K. and overseas universities for undergraduate, postgraduate, and research degrees. He is also a successful Entrepreneur. He is the Head of Enterprise at the Faculty of Engineering and Technology. He has been awarded various commercial and research grants, nationally and internationally, over 5M from overseas research and educational partners, U.K., through British Council and directly from industry with portfolio of various knowledge transfer programs between academia and industry. He has been the Founder and the General Series Chair of the IEEE International Conference on Developments in eSystems Engineering DeSE (https://dese.org.uk), since 2007. He has been actively involved as a member of editorial board and a review committee for a number peer-reviewed international journals. He is on a program committee or as the general chair for a number of international conferences. In December 2020, he was promoted and appointed by The Queen to the Most Excellent Order of the British Empire, OBE—Ordinary Officers of the Civil Division of the said Most Excellent Order for the Services to Scientific Research.

● ● ●